Toward Actuation of Kresling Pattern-based Origami Robots

Kejun Hu [*1], **Thomas Jeannin** [1], **John Berre** [2], **Morvan Ouisse** [1] **and Kanty Rabenorosoa** [1]

[1]Université Bourgogne Franche-Comté, FEMTO-ST Institute, CNRS/UFC/ENSMM/UTBM, Besançon 25000, France
[2]Université de Strasbourg, ICube Laboratory, CNRS/US/ENGEES/INSA-Stras, Strasbourg 67000, France

E-mail: kejun.hu@femto-st.fr

July 2022

Abstract. This work investigates the technical requirement for the actuation of the bi-directional rotational motion (BRM) of engineering-material-based non-rigid origami robots. While the vast majority of previously published results have focused on paper-based origami structures driven by translation-motion, polypropylene (PP) is implemented in this research to investigate its ability to respond to engineering requirements according to BRM. Following this objective, three experiments are proposed to identify the technical performances of PP-based origami and kirigami robots based on Kresling pattern. First, the stabilization test shows that two hundred full folding cycles are required to reach a repeatable mechanical response. Second, the BRM test characterizes the various mechanical performances of both origami and kirigami structure: the polypropylene(PP)-based origami outperforms existing structures in the literature. Third, the actuation test shows that the actuation mechanical requirements can be described using three key parameters: the required torque for folding, the shape-blocking stiffness, and the bistable portion. Finally, in order to support the development of PP-based origami/kirigami robots, a 'Bar and Hinge' reduced-order model is implemented for the description of the nonlinear hysteretic behavior and bistability. This method constitutes a useful tool for the design of highly nonlinear/bistable engineering structures based on PP origami and kirigami.

Keywords: Kresling Origami, Kirigami, Actuation, Bi-Stability, Origami robots

1. Introduction

Origami and kirigami provide a means of transforming thin tessellated panels into 3D form with many unique and desirable structural properties such as auxetics, tunable stiffness, and multistability [1]. These materials and structures have promising applications in various domains, including biomedical engineering [2], acoustics [3], aerospace [4], biomimetic engineering [5], fold-core structures [6], metamaterials [7],

or robotics [8]. Especially, robots inspired by folding mechanical structures known as 'Origami robots' gained much attention recently [9]. As for the robotics field, the introduction of origami engineering enables 'semi-rigid' properties. In other words, they exhibit the properties of both rigid and soft robots [10]. However, the increasing applications of origami robots require designers to accurately understand the mechanical behavior of folding structures. Generally, origami structures are classified in two categories: rigid-origami and non-rigid origami [1]. The former is usually considered as a linkage mechanism in which the folding crease behaves as a perfect rotating hinge with negligible elastic stiffness. The panels are assumed to be rigid [1, 11]. This assumption has been proven useful to describe the folding kinematic of various structures [12]. However, the assumption can be violated when the deformation on the panel and crease is not neglectable. In a physical system, the folds have a torsional stiffness, and the panels can deform. Moreover, if the origami crease pattern supports a nonconvex energy landscape, multiple stable states manifest, thus gain additional degrees of freedom from non-negligible strain of panels and expend the functionality of the structures [13]. For example, a gripper based on a Miura-ori pattern is capable of maintaining its open or closed state without external load [14]; an earth-worm like robot based on a water-bomb pattern can change its diameter and length in a bistable manner [15]. It is worthing to remind that, the choice of the pattern, materials, and actuation system cannot be decoupled when designing an active-origami structure [16].

Table 1: A summary of well-known origami patterns and corresponding characteristics. Beyond other basic origami patterns, the **Kresling tower** exhibits unique mechanical properties such as translation-rotation coupling and multi-stablility while removing the rigid-foldability. This table is inspired by [17, 18].

Pattern	Rigid foldability	1-DOF	Flat foldability	Multistability	Auxetics
Miura-ori	Yes	Yes	Yes	Yes	Yes
Waterbomb	Yes	Yes	No	Yes	No
Diagonal/Yoshimura	Yes	Yes	Yes	No	No
Accordion	Yes	Yes	Yes	No	No
Flasher	Yes	Yes	No	No	No
Kresling	**No**	**Yes (coupled)**	**Yes**	**Yes**	**No**

Besides others known origami patterns (see table 1), a system named 'Triangulated Cylinder' [19] or 'Kresling tower' [20] earned attention in the last decade[21], thanks to its unique properties. Structures based on this pattern exhibit one DOF with coupled rotation and translation leading to helical motion, with a highly nonlinear hysteretic behavior, and its rigid foldability is completely removed [17]. These properties were used for various goals such as mechanical bit memory switch [22], medical instrument support system [23], and vibration absorption [24]. Especially, since the shape-changing can be performed using actuation in a repeatable and programmable manner, the Kresling tower has been proven to be an excellent candidate for active-origami-based robots. For example, [25] introduces a 150 mm length crawling robot consisting of two Kresling

towers and a bending origami bellow. Driven by two servo-motors, the prototype is capable of crawling at a velocity of 11.8mm/s. Using a similar actuation strategy, [26] introduces a tendon-driven robot-arm that exhibits the desired reconfigurable articulation behavior. The system consists of three pairs of Kresling towers in series that can provide tunable local bending stiffness according to the structure's bistable behavior. [27] introduces a system that is capable of untethered and local distributed multimodal actuation with controllable speed. The goal is achieved by coupling of geometrical and mechanical properties of the bistable Kresling pattern with a magnetically responsive material. A similar structure can be found in works of [28], in which the prototype's deployment is achieved using shape-memory-alloy based actuators. [13] provides a soft robot arm with omnidirectional twisting and bending under pneumatic actuation in a pre-programmable manner. The complex motion is attained by a series of Kresling towers with eccentric bi-stability and is piloted by a 'loading-path' depending controller. Currently the most popular actuation strategy is to directly use conventional actuators such as servo-motor, air pump or magnets. Even though these actuators are easy to integrate, the relatively low power density, the relatively large stroke requirement, and large space requirement become challenging for down-scaling applications.

Generally, the Kresling tower consistently exhibits hysteretical behavior with multi-stability when subjected external loads. Many efforts have been made to describe this complex behavior, usually using either a finite element-based approach or a lattice framework-based approach. The former refers to a discretization of a continuous origami structure using sheet elements based on the assumption that the thickness of the folded sheet is small compared to the overall-size [28, 16]. However, although accurate and capable, the finite element approach requires a high computational cost. The latter can be considered as a simplified version of the aforementioned approach, which assumes that only simple bending occurs on a panel. As indicated in [29], this reduced degree-of-freedom model can provide accurate prediction while being computationally efficient. Previous studies show that the assignment of linear tensile stiffness is capable of describing the quasi-static [30] and the dynamic behavior [31] of Kresling tower. Through this method, [32] introduces a detailed qualitative study of the potentials concerning the translation-rotation-coupling during shape-changing and highlights the advantages of pure rotational actuation. As indicated by [33], this method has limitations in the description of quasi-static mechanical response during folding. It is worthing to remind that a 'bar and hinge' reduced-order origami simulator named *Merlin2* [34] is frequently mentioned and found useful for the description of paper-based Kresling tower's behavior [35, 27, 26]. However, most of the current research work on this topic is usually performed using paper, which is easy to be folded but exhibits very weak properties in term of shear stress, and can be easily teared [18]. Although, a few works have been carried out to study the performance of engineering material-based Kresling tower [15, 22, 26, 36, 37], largely the works are based on the fabrication and realization of such folding structures. Thus information that relies on actuation system cannot be found in the literature. Indeed, a complete study for structure's mechanical behavior is

necessary for identification of technical requirements for 'self-actuation' origami.
Regarding the experimental characterization of Kresling tower, an imposed translation motion/strain driven 'folding' or 'folding-deployment' test is usually carried out for characterization (see table 2). Especially, the tests require the release of the coupled rotational dof during the test. Based on this condition, a variety of methods were carried out: the rotation can be released using a ball joint [38], a slide plate [27], a bearing mechanism [33, 28], or it can be neutralized using two symmetric towers [22]. However, the rotation induced by the 'Snap-through' effect can not be controlled. Thus the moment of inertia of the origami supports affects the mechanical response of the structure. To overcome this problem, the test needs a rigorous controlling of the coupled rotational and translation degrees of freedom in a quasi-static manner. Moreover, BRM-based actuation reduces actuation requirements in terms of actuation stroke and operational space compared with translation mode, while it has not been investigated in detail. Table 2 summarizes the available experimental data of Kresling pattern-based origami/kirigami structures in the literature. Their mechanical performance and corresponding characterization methods are compared to the PP-based Kresling tower analyzed in this work. While the available origami face challenges in the way discussed earlier, the PP-based Kresling tower proposed here outperforms existing structures.

The objective of this article is to establish a method based on experimental

Table 2: Kresling towers properties available in literature

	Samples		Charaterization		Geo parameters [1]						Mechanical performance			
Year	Mat	Type [2]	Test [3]	Cycling	n	R (mm)	b/R		l/R		TF (N) [4]		BP/R [5]	
1996 [38]	Al-alloy[6]	O	F	No	8	65.38	-	0.76	-	1.38	-	15	-	-
2018 [28]	paper	K	F-D	Yes	7	38.5	1.30	1.57	1.70	1.78	2	4	0.94	1.30
2019 [33]	paper	O	F	Yes	6	-	1.30	1.50	1.89	2.03	2.12	2.87	0.50	0.78
2019 [39]	paper	K	F-D	Yes	8	39.20	1.30	1.68	1.78	1.96	2	5	1.02	1.27
2020 [27]	paper	K	F	Yes	6	13	1.33	1.61	1.89	1.98	0.16	0.9	0.50	0.84
2021 [22]	PET	O	F-D	No	5	13.61	1.22	1.44	1.92	2.20	0.9	3.4	1.18	2.03
This work	PP	O & K	F-D	Yes	8	30	-	1.87	-	2.17	-	22.6	-	0.57

[1] n: polygon silde number; R: circumscribed radius of the polygon. The two rows represent bounds of corresponding parameter
[2] O: origami; K: Kirigami for the structure type
[3] F: folding test; F-D: folding and deployment test
[4] TF: threshold force
[5] BP: bistable portion
[6] The panel are in Al-alloy and the crease are in Irathane

and numerical analyses to determine the technical requirements of a 'self-actuation' origami robot based on Kresling tower made with engineering materials. Two well-known structure types are considered: origami and kirigami (see table 2). The main contributions of this paper are: 1) development of charaterization method of an engineering-material based Kresling tower in origami and in kirigami states, 2) quantitative description of structure's highly nonlinear folding and deployment behavior in a quasi-static manner, and 3) identification of technical requirements for BRM-based actuation of meso-scale origami robots. Specifically, the remainder of this paper is organized as follows: Section 2 details the study's material and methods in terms of numerical and experimental analyses of the structure. Section 3 details the

results of experimental test, and provides a method of actuation technical requirements construction using a numerical approach. Conclusions are drawn in section 4.

2. Materials and Method

The design, fabrication, and characterization method are presented in this section. The geometrical design method is provided using four independent geometrical parameters. Both experimental testing and numerical modeling are used to identify the actuation technical requirements of an engineering-material-based non-rigid structure. Three tests for the experimental characterization are proposed to cover the main features required for the design. Finally, a numerical procedure implements a reduced-order 'bar and hinge model' and the model parameter identification process is presented.

2.1. Materials, design and fabrication

The use of paper to realize origami can present phenomena of delamination or tearing leading to a premature wear of the structure. In the literature, the polymers such as polyethylene terephthalate (PET) [37] or polypropylene (PP) [40, 41] are commonly used for robotic application. Some polymers can be cut by laser, then glued, thus presenting the same manufacturing advantages as paper. In [42], an experimental protocol measuring the performance of material to realize the kinematics of a pin joint indicates that PP has the best result among tested polymer. Based on this study and its previous use, PP has been selected as the material for this study.
Generally, a Kresling tower is built by taking a thin flat foldable material and tessellating it into n parallelograms each composed by two similar triangles. The relevant geometrical parameters in the literature of a Kresling tower are given in figure 1, where R denotes the circumscribed radius; H_i the tower height at stable states; ϕ_i the relative rotation angle at stable states; a the polygon side length; l, b and c the diagonal length, the side length and the height of parallelograms, respectively. $\lambda\theta$ is the angle between l and a with λ the planar angle ratio and θ the angle between the radius and the polygon side, respectively. Four independent geometry parameters are required to geometrically determine the configuration of a bistable Kresling tour. Table 2 presents the existing experimental data using a set of variables (n, R, b, l) that are converted from the data in the literature. As shown in figure 1 c), the origami part is shaped from a 0.5 mm thick PP film using a Trotec laser cutting machine. The design method introduced in [40] is used to obtain the set of geometrical parameters for the 2D pattern. To this end, a set of four parameters according to the 3D configuration in terms of (n, R, H_1, H_2) are considered. Practically speaking, the tower is composed by two regular octagons with $R = 30mm$ radius with two stable heights $H_1 = 29mm$ and $H_2 = 54mm$. The corresponding 2D pattern parameters are shown in table 2. In this study, origami and kirigami towers sharing the same geometry configuration are considered (see figure 3a). The origami configuration corresponds to a tower without cutting, while kirigami

refers to a tower where the mount folds have been cut, as is the cases mentioned in table 2. The pattern is designed with dashed lines to realize fold lines [40]. These dashed lines are configured with a 1:1 stroke rate and the width corresponds to the minimal laser spot (around 0.3mm diameter). Besides the kirigimi type Kresling tower that completely releases the mount crease, the origami type sample requires a gluing operation to obtain a closed cylindrical-form structure. Gluing tabs are therefore added to the pattern, minimizing their surface to limit the overlap on the gluing areas [40]. Then these tabs are prepared, they are sanded and degreased before a surface plasma treatment by corona effect. Finally, blocking tabs with circular holes are realized to ensure reproducibility in the positioning of the tower.

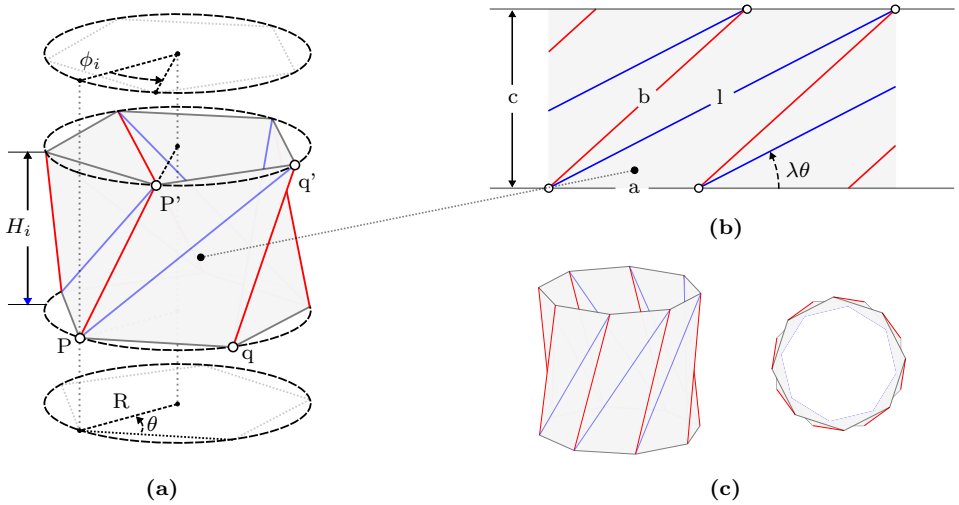

Figure 1: An example of modular Kresling origami: a) geometry of the Kresling tower for n = 5, b) zoom of Kresling tower in 2D flat state, c) geometrical configuration investigated in this work.

2.2. The constitutive model

The *Merlin2* [34] is adopted in this study because of its relatively high accuracy and high efficiency in predicting the quasi-static folding behavior. This model is based on the formulation of the total potential energy (Π) using a set of independent state variables ($\mathbf{u}$,$\mathbf{f}$), where $\mathbf{u}$ presents the displacement and $\mathbf{f}$ presents the external force. The total potential energy accumulates the strain energy relying on stretching of panels edges and hinges (U_S), bending of hinges (U_B), and folding hinges (U_F). The explicit form of the total potential energy is given by

$$\Pi(\mathbf{u}) = U_S(\mathbf{u}) + U_B(\mathbf{u}) + U_F(\mathbf{u}) - \mathbf{f}^T\mathbf{u} \tag{1}$$

Using virtual work principle, the equilibrium is obtained when the sum of potential energy according to each of its individual parts becomes zero. *Merlin2* uses nonlinear constitutive laws since linear elastic models do not accurately describe the observed material behavior. For stretching bars, an Ogden hyperelastic model is implemented.

For folding hinges, a rotational spring with a tangent equation form elastic constitutive model is considered to describe mechanical behavior of creases and small bending on the panels. This results in a reduced-order model that enables the description of the complex folding kinematics and advanced mechanical behaviors of non-rigid origami. The construction of the numerical model is presented in the following subsection.

2.2.1. Numerical model and parameter identification The numerical model, implemented in *Merlin2* consists of panels joined together by torsional bars along the fold creases. The model parameters that are assigned are shown in figure 2b. This reduced-order approach provides two types of torsional elements: the folding bar elements and the bending bar elements. The former relies on the folding crease with relatively large twisting angles, the latter is usually carried out to describe bending on the panel. As reported in [28, 33], such elements are useful for describing the bending on non-triangle panels, thus are capable of capturing complex behavior such as kinking or degradation on the crease. Regarding the current geometrical design, the pattern is already tessellated in triangle panels, and no kinking behavior has been observed during the study. Thus the bending behavior is neglected in this case, and it is assumed that all the deformation is induced either by the stretching of panels or the folding of creases. The torsional bars follow a non-linear torque-angle relationship with a user-defined stiffness constant of K_f. Besides the torsional element, the truss elements adopt an Ogden-2 material model for hyperelastic behavior.

As shown in the equation 2 and 3, this three-parameter model is configurated using three parameters: C_0, α_1, α_2 representing respectively the initial tangent modulus, the first material constant, and the second material constant.

$$S_X = \sum_{j=1}^{2} \mu_j \lambda_j^{\alpha_j - 2} \tag{2}$$

$$C_0 = C(\lambda_1 = 1) = \sum_{j=1}^{2} \mu_j \alpha_j \tag{3}$$

Since the mountain crease are tailored for two types, the relevant tensile stiffness and torsional stiffness are different. Two parameters $\beta_1 = K_s^m/K_s$ and $\beta_2 = K_f^m/K_f$ are used to capture the influence of opening on the axial stiffness and torsional stiffness. Regarding the boundary conditions and loading, all the dofs at the bottom of the structure are constrained (black arrows in figure 2a), and an imposed axial displacement is applied on the degree of freedom in the transverse direction on the top of the structure (magenta arrows in figure 2a). An imposed displacement path is defined as 0% to 60% of tower height in incremental form. The equilibrium path is investigated using a modified generalized displacement control method (MGDCM)-based solver to describe the snap-through and snap-back behaviors [34]. Moreover, the torque-angle experimental curve can be converted into equivalent force and displacement using the derivation of the stored energy. The model is therefore updated using an optimization algorithm to identify model parameters based on the experimental results. To this end, a nonlinear

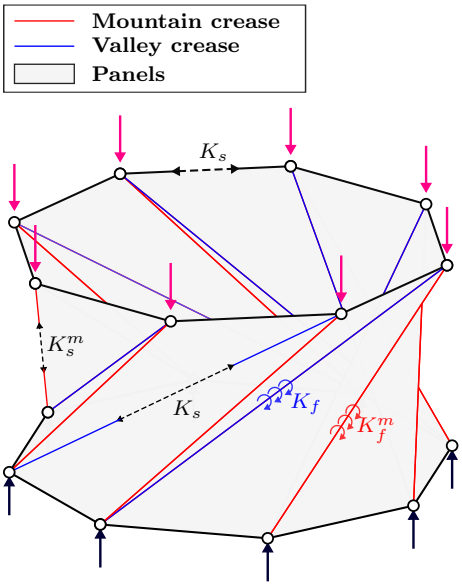

(a)

Model parameter	
C_0	initial tangent modulus
α_1	first orgden-1 model constant
α_2	second orgden-1 model constant
A	truss section area
β_1	area ratio for mountain crease
β_2	stiffness ratio for muntain crease
K_s	truss axial stiffness
K_f	torsional stiffness
K_s^m	truss axial stiffness for muntain crease
K_f^m	torsional stiffness for muntain crease

(b)

Figure 2: Numerical model used for Kresling tower in PP: a) illustration of the nonlinear bar-hinge model, where dash lines in black color represent the stretchable truss elements, blue solid lines correspond to the valley creases, and solid lines red are the mountain creases; b) model parameters for the nonlinear bar-hinge model.

least-squares optimization method using a 'Levenberg-Marquardt' algorithm is carried out for parameter identification.

2.3. Experimental characterization

The design of actuators requires a delicate understanding of the structure's mechanical behavior. The Kresling towers exhibit a translation-rotation-coupled motion and a bistable behavior during shape-changing. Moreover, the mechanical response of origami is sensitive to factors such as material properties and geometric design [1]. For example, the torsional stiffness of rigid origami can be alternated by tuning the thickness of the single folding joint [43]; the folding response of a paper-based Kresling tower can be adjusted between monostable and bistable behavior by tailoring the geometric parameters [44, 33]. Consequently, the response of the Kresling tower under various of mechanical conditions has been thoroughly characterized. Three tests are proposed to investigate the technic requirements of the engineering-material-based Kresling tower: 1) a cyclic test to identify the necessary cycle number for initialization of structure, 2) a bidirectional rotation motion (BRM) test for the characterization of the structure's quasi-static behavior, 3) an actuation test for characterization during shape-changing.

2.3.1. Benchmark and test routine The experimental setup consists of an aluminum frame that integrates two rigid plates. The bottom plate connected with support is

fixed with the force cell of an Instron tensile machine (Instron 2530-1KN, 0.001% for full range on measurement). The top plate is movable and is controlled by the tensile machine (Instron electropulse E-10000) (see in figure 3a). The machine can provide a 'translation-twisting' motion while sensing the response with a certain velocity. Both plates are attached to the machine with metallic clamping tools to avoid errors during the state transition. Acrylic plates with a hole of the same shape as the according octagon; thus, the blocking tabs are tightened using screws to ensure reproducibility of the position state of each sample (see figure 3a). The tensile machine has measure limits such as 60mm for translation and 32π rad for rotation. An example of test

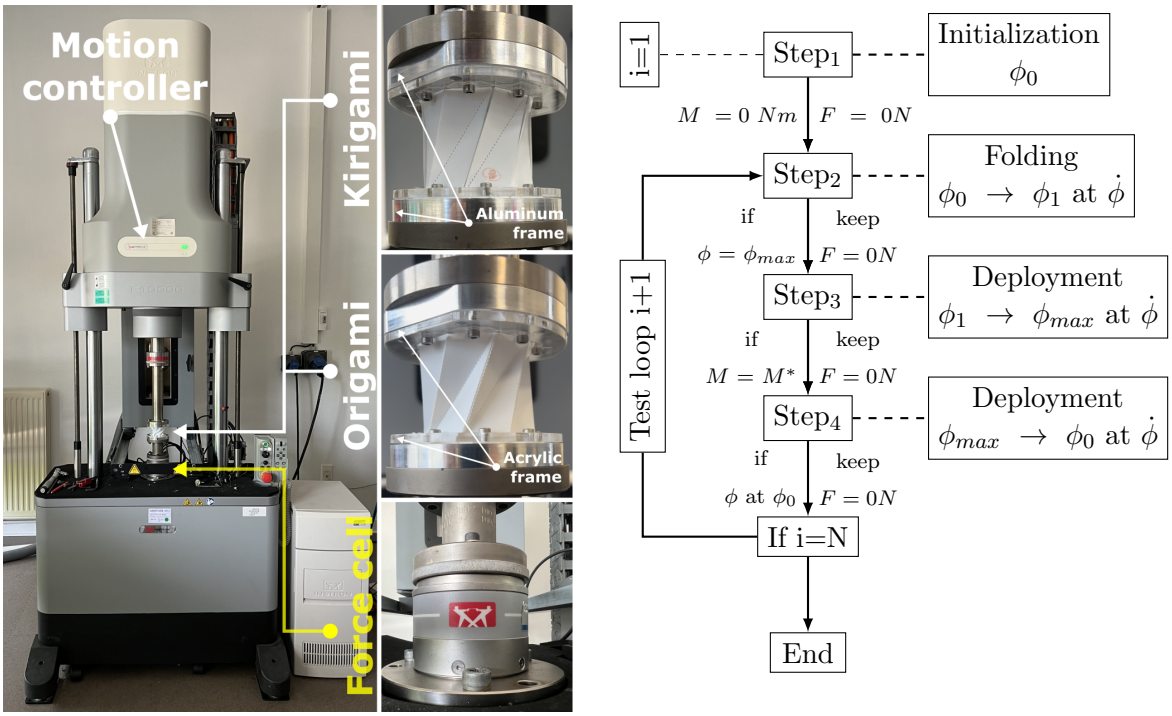

(a) (b)

Figure 3: Benchmark and test routine: (a) An example of Kresling tower characterization experimental setup, a sample (origami or kirigami configuration) is attached between the aluminum plates using screws. A pair of acrylic plates are embedded to ensure the boundary conditions of the tower; (b) An example of test routine of a BRM-driven test of Kresling tower.

routine is shown in figure 3b. $\phi_0, \phi_1, \phi_{max}, \dot{\phi}, F, M, M^*$ are the reference rotation angle, the intermedia angle around the state transition during deployment, the maximum angle during folding, the rotation rate, the axial reaction force, the axial reaction torque, and the maximum reaction torque, respectively. The base of the tower is fixed. The rotation angle of the top of the tower is imposed by the machine. In order to allow the free translation motion in a quasi-static manner, the vertical reaction force is regulated at 0 N. Hence, when the top platform is rotated clockwise, the distance between the two

plates is reduced, and the required torque for twisting can be recorded accordingly. Once the structure has been fully folded ($step_3$), the test is reversed and a deployment motion can be performed. The test is carried out in a cyclic manner, and the cycle number is determined regarding the test objective that will be presented in the following. It is worthing to remind that the structure stiffness largely changes due to the 'snap-though' effect, and the outbreak of the state transition evolves during the cycling. Using a zero reaction torque detection during the deployment process can help the machine to achieve accurate motion control.

2.3.2. Origami behavior stabilization Regardless of the particular material parameter being characterized, one must always consider the importance of material history dependence that affects the origami's behavior. When a new origami structure is subjected to a load path in a repeatable manner, the mechanical response will generally change with each cycle during a certain number of cycles before being stabilized. For example, a Kresling tower in paper needs more than 300 cycles to be stabilized [27], and similar observations for single folding hinge using engineering materials have been reported in [42, 45]. Regarding the non-rigid origami in engineering material such as PP, no existing test routine can be found in the literature. A test routine with controlled two-dofs motions is performed in a cycling manner. A sample that is closed to the kirigami configuration is tested using a cycle number of one thousand to detect the necessary cycle number for stabilization. In this case, the tower is subjected to bi-directional rotation with a stroke of $\pm$ 80 degrees at a constant rotation rate of $5°/s$. The reference angle is defined according to the initial equilibrium state of the tower at unfolded state.

2.3.3. BRM test A BRM test is carried out to characterize the bistable behavior of the Kresling tower in PP. As shown in figure 3a, a load cell is used to record the reaction torque of the sample during folding and deployment. The aforementioned test indicates that the structure needs a certain cycle number to reach a steady state. Therefore, to ensure the repeatability of results, all the samples are subjected to the detected cycle number as a pre-conditioning. Four stabilized samples, including two samples for origami and kirigami configurations are then characterized using the aforementioned routine. Each sample is subjected to thirty cycles of BRM-driven imposed rotation with a constant rotation rate of $\pm 4°/s$. However, since the compliance of the kirigami samples is larger, a rotation rate of $\pm 1°/s$ is applied to ensure the control accuracy, thus providing three times more data using the same acquisition frequency (see in table 3). The experimental data are then processed using a high-order polynomial interpolation method to compare with the aforementioned bar-hinge model. As shown in figure 4, seven properties are selected to characterize the structure's performance:

- The hysteresis Γ corresponding to the dissipated energy according to one fold-deployment cycle (the grey area in figure 4).

- Threshold efforts during shape changing $M_{fold}, M_{deploying}, M_{H_{max}}$, where M_{fold} is the folding threshold effort, $M_{deploying}$ is the deploying threshold effort, and $M_{H_{max}}$ is the effort that corresponds to a maximum imposed position after a full folding.
- The bistable portion $BP = \phi_2 - \phi_1$. ϕ_1 corresponds to the position that refers to the folded stable configuration, ϕ_2 is the position that refers to the deployed stable configuration.

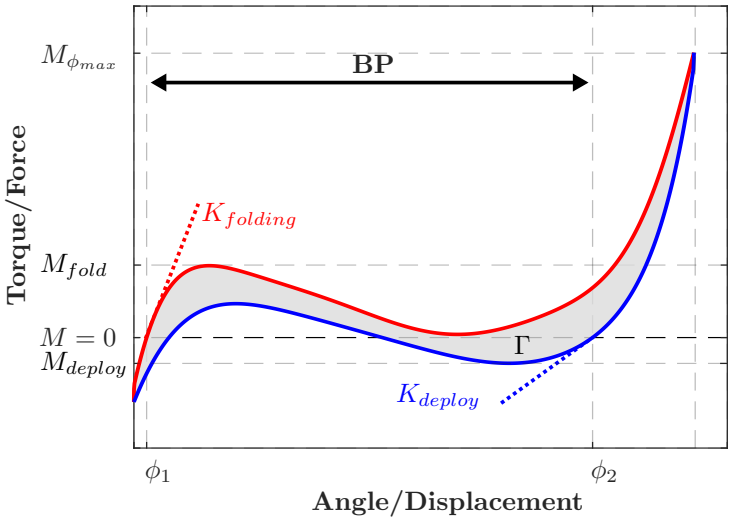

Figure 4: An example of different mechanical properties of a PP-based modular Kresling tower. The red curve presents the folding mechanical response, and the blue curve presents the deploying mechanical response.

2.3.4. Actuation test The objective of the actuation test is to characterize the origami's response regarding different actuation states. In this case, a displacement-based BRM actuation test with varying rotation angle is applied on a Kresling tower in origami configuration. The test is carried out using the same setup as the previous section but a different test routine. The course is applied at a rotation rate of 4 $°/s$, and the test is repeated four times for each angle. Six angles that belong to 50% and 90% of the bistable portion of the origami are investigated by the BRM test.

3. Results and discussion

3.1. Origami behavior stabilization

The torque-angle relationship of the origami stabilization is shown in figure 5. Each color correspond to different cycle numbers, ranging from one to one thousand. The evolution of global stiffness due to cyclic loading can be observed. The evolution of the response between the first and the one thousand-th cycle is observed. It is trivial

that the cycling induces a large deviation of the structure's shape-changing behavior. Large variations in terms of criteria torques and localization of stable positions induced by the stabilization effect are observed. For example, a 67% reduction of M_{fold}, a 52% reduction of M_{deploy}, 57% reduction of hysteresis, a 62% reduction of K_{fold}, a 59% reduction of K_{deploy} and a 50% increase of $M_{\phi_{max}}$ are observed. An influence on bistable portion is detected as a 13% reduction that mainly induced by a shifting of ϕ_2 is found. The torques during folding and deploying are therefore selected to detect quantitatively

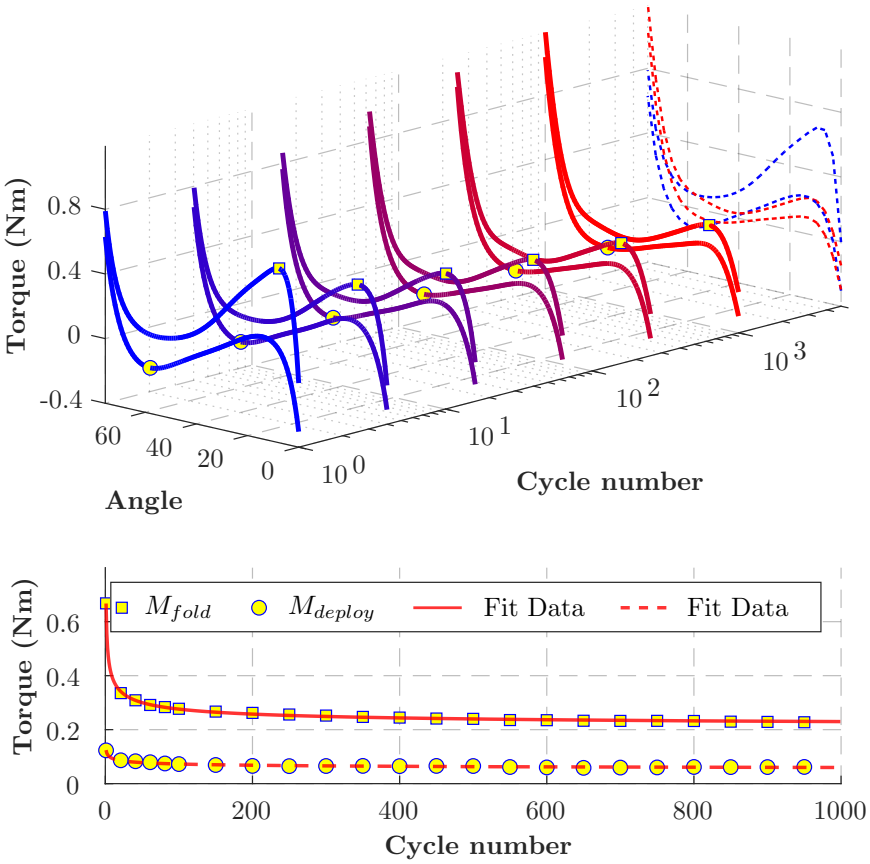

Figure 5: Investigation of the stabilization of the mechanical properties during multiple BRM cycles: one thousand cycles at constant rotation rate are applied. The solid lines correspond to the cyclic mechanical response. The dashed lines compare the results according to the first and the last cycle. The reaction torques are captured to evaluate the response evolution: the mechanical response stabilizes around 200 cycles.

the necessary cycles for folding behavior stabilization. The evolution in shown in the bottom part of figure 5. Comparing the torque for first and one-thousandth cycle, a reduction of 67% for folding and a reduction of 52% for deployment are observed. The response according to the first cycle yields a considerable difference compared to subsequent cycles. As shown in the figure, these experimental data can be interpolated using a two-term power series model. It is worthing to remind that the derivative of

these functions achieves almost zero when the cycle number is close to 200. It is also observed that the threshold torque always occurs during folding, and the ratio becomes constant after stabilization. Additionally, none of panel kinking nor degradation had been observed on the structure after one thousand cycles. Consequently, the evolution can be explained by the contribution of the formation of folding creases. Regarding the behavior after stabilization, the tower requires 0.3Nm as threshold torque (M_{fold}) to achieve the shape-changing, while the initial value was 0.7Nm. Regarding the same rotation angle, the maximum torque according to ϕ_{max} increases from 0.65Nm to 1.2Nm. It is worth to remind that the threshold torque during folding is three times larger than during deployment. Assuming that an actuator provides similar output power in two directions, maximum torque during folding M_{fold} can be used as a criteria value for the actuation technical requirement.

3.2. BRM test

The torque-angle relationship of the stabilized Kresling tower is shown in figure 4. Globally, both types of Kresling tower exhibit a bistable behavior with hysteresis: during folding, the torque first increases until reaching a threshold value; after attaining this value, the structure snaps, yielding a negative stiffness. The torque thus decreases to a minimum value according to a nonzero local minimum potential energy state. Then, the structure strengthens with continued fold induced by monotonically increasing torque. Therefore, only one zero-torque point can be observed during folding according to the unfolded state. On the other hand, the structure exhibits three zero torque points during deployment. Regarding the deployment process that begins from a full folded state at the maximum imposed rotation angle, during the load release, the structure recovers its equilibrium with relatively high and quasi-constant stiffness. Thus a first equilibrium point is obtained. If the twisting is continued, the structure induces a typical bistable behavior: the structure attains maximum potential energy at the second zero torque point. It then achieves its second equilibrium point according to its unfolded state. It is worthing to mention that the coupling between rotation and transverse displacement is different between origami and kirigami configurations. The displacement-angle relationship during thirty cycles are shown in figure 6. The coupling of origami exhibits a quasi-linear relationship, while the one induced by kirigami is nonlinear. The angle $\phi \in [0, 78]$ degrees can be fitted using a function of displacement $w \in [0, 25]$ mm that is given in table 3. It is trivial that the linear function is sufficient to describe the coupling between angle and displacement for origami, while a kirigami needs a quadratic function for the fitting. The structures are demonstrated capable of providing a volume reduction ratio up to 50% upon a pure twisting actuation. The torque-angle relationship for PP-based Kresling towers are summarized in figure 7. Additionally, using a origami structure as a reference for comparison, modifications of the structure's mechanical performance that are induced by the releasing of the mountain creases are observed (see table 4):

(i) The hysteresis is reduced with a ratio of 50%.

(ii) The stiffness decrease according to folding and deployment has been observed. Compared to the origami, the stiffness of the kirigami is reduced by a factor of 3. it is worth reminding that the distinction of stiffness according to two stable states is well observed.

(iii) The threshold torque during folding is decreased with a proportion of 64%.

(iv) A 10 % reduction of bistable portions has also been observed regarding the same test conditions.

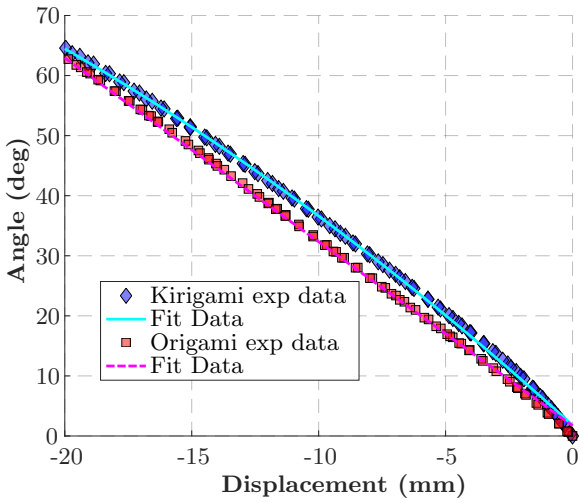

Figure 6: Summary of coupling between displacement and rotation for different types of origami: diamond markers present the experimental result for kirigami, and square markers show the experimental result for origami.

Table 3: BRM test results: Coupling of rotation and displacement for stabilized Kresling tower.

	Polynomial order	Polynomial coefficients[2]			R	DOF Adjusted R-Square	RSME [1]
Origami	1		-3.0532	1.8676	0.9989	22745	0.7124
Krigami	2	-0.044	-4.0521	-0.2898	0.9994	90247	0.5398

[1] Polynomial coefficients ordered by descending powers

[2] Root Mean Squared Error

Briefly, the release of mountain creases induces a modification in the Kresling tower's global mechanical characteristics in terms of hysteresis, shape-blocking stiffness, threshold torque, and bistable portion. Moreover, the distinction for threshold torque and stiffness relying on the folding and deployment are observed. The folding of the structure requires globally 60% higher actuation torque than for deployment. It is worthing to indicate that the development of an origami robot usually needs to

consider two requirements: shape-changing robustness and actuation conditions (limits for actuation effort and stroke). These two requirements are sometimes contradictory. A higher shape-changing stiffness induces a robust folding process, but meanwhile, the increase of actuator performance reduces the structure's deformability. Therefore, the trade-off needs to be addressed during the robot design.

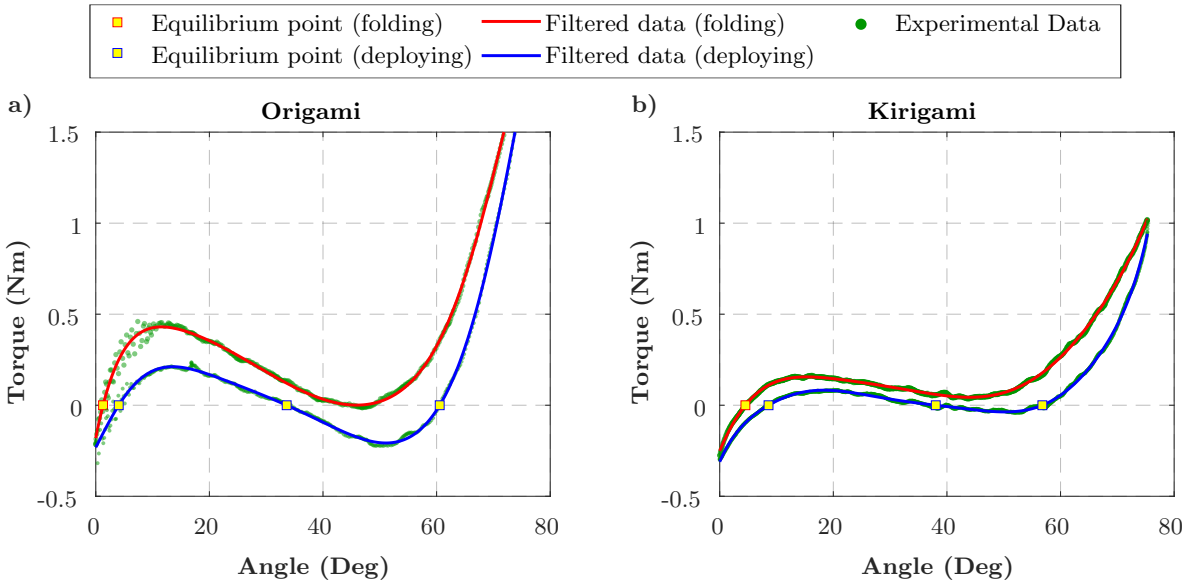

Figure 7: Torque-angle relationship of stabilized Kresling towers: the green dots present the original experimental data of different samples according to a) origami and b) kirigami. The solid red lines illustrate the filtered data during folding, and the solid blue lines show the filtered data during deployment. The yellow markers show the equilibrium points during the shape-changing.

Table 4: Summery of different mechanical performance of PP-based Kresling tower

Unit	Γ J	M_{fold} Nm	K_{fold} Nm/rad	K_{deploy} Nm/rad	$M_{\phi max}$ Nm	BP deg
Origami	0.297	0.430	6.938	2.934	1.878	59.26
Krigami	0.152	0.156	2.203	0.700	1.101	52.38

3.3. Actuation test

Figure 8 summarizes the actuation test results with six different actuation loading angles. The grey points present the experimental data of all test cycles, the solid lines in red correspond to the filtered folding response, and the solid blue lines show the filtered deployment response. The structure exhibits a hysteresis loop behavior according to different actuation angles. It is clear that the location of the equilibrium point according to folded state relies on the folding history. For different actuation

loading angles, repeatable and distinct folded conditions are observed. The structure requires to be activated with a sufficient torque (above the threshold torque) and sufficient ending activation angle (above 50 degrees) to achieve the folded stable state. Otherwise, the structures exhibit monostable behavior during shape-changing even if the criteria torque is attained. Hence the characterization requires an actuation angle large enough to ensure the observation of bistable behavior. On the other hand, a shift of the folding state position is observed. The maximum load angle can explain this phenomenon during folding. After attaining a loading angle (above 50 degrees), the structure recalls its stable folded state in a quasi-elastic manner. Therefore, the localization of folded states becomes predictable. Moreover, the origami Kresling tower provides a linear coupling between displacement and angle. Consequently, graphical methods or asymmetric algebraic models that are constructed using experimental data (for example, a minor hysteresis loop model [46]) can be utilized to achieve a specific folded state.

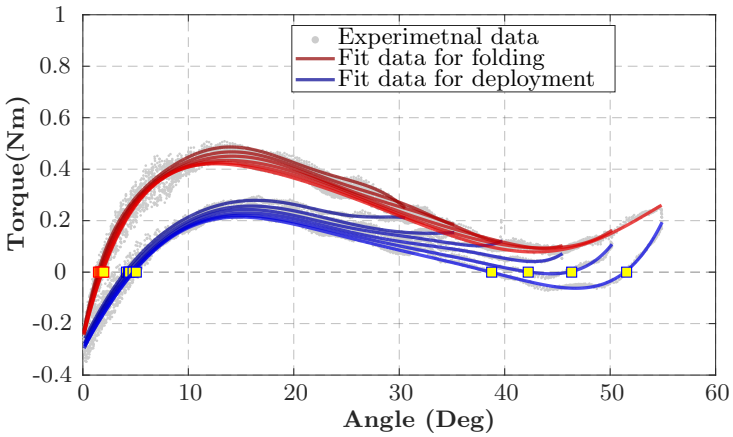

Figure 8: The experimental results of actuation test with six final folding angles in a cyclic manner. The red solid lines present fitted data for folding and the blue solid lines present the fitted data for deployment. Minor hysteresis loop form torque-angle relationships are observed.

3.4. Parameter identifications using bar-hinge approach

The experimental data of the BRM test are translated to force-displacement relationships using the derivation of the strain energy. Therefore, the criteria torque for folding, the folding stiffness, and the first stable point deployment are converted to a set of equivalent force F and displacement information U and then used as a reference for the optimization (see section 2.2.1). For material parameter of PP, the parameters are identified with equation equation 2 and 3, using the tensile results reported in [47]. The three parameters are defined as $C_0 = 0.5GPa$, $\alpha_1 = 0.5$, and $\alpha_2 = 1$. The four-parameter-based optimization is launched to determine each parameter's variation

interval The results shows that the bar section area A and the torsional stiffness constant k_f converges to a constant set of value of $A = 1.65e-6m^2$ and $k_f = 0.06\frac{Nm}{rad \cdot m}$. The optimization results are summarized in table 5. The model is shown to be able to provide an accurate description of all the aforementioned technical requirements of an actuator, such as criteria force during folding, bistable portion, and folding stiffness. However, one needs to indicate that discrepancies are observed according to deployment stiffness. The model provides obvious underestimations for deployment stiffness compared to the experiment while the evolution tendency is correct. This discrepancy probably originates from the contact between panels and high-nonlinear folding behavior using thick material. To investigate the effect of material properties, a simulation is performed with the same geometrical design using paper's material parameters. These parameters are identified by [27] on a series of paper-based kirigami type Kresling towers with $c \in [16.66, 20.99]$ mm with constant R (see table 2). The comparison shows that the induction of PP provides large increases in mechanical performance while the bistable portion is at the same level. Especially, the Origami configuration provides even twenty-times larger stiffness and ten-time larger criteria force than the kirigami.

Table 5: Summary of BRM test results of Kresling tower using different material. The model is shown able to provide an accurate prediction of technical requirements for shape-changing.

Type Material		Origami PP	Kirigami PP	Kirigami paper
Model parameter	β_1	1	0.220	0.5
	β_2	3.416	2	0.01
Criteria force (N)	Experiment	22.57	8.188	-
	Simulation	22.78	9.518	2.2194
Bistable portion (mm)	Experiment	19.42	17.10	-
	Simulation	20.81	19.89	21.3125
Folding stiffness (N/mm)	Experiment	13.42	4.595	-
	Simulation	16.06	4.958	0.6235
Deployment stiffness (N/mm)	Experiment	8.486	2.295	-
	Simulation	2.888	1.274	0.2590

Regarding the folding process of structure, figure 9 shows a simulation result using identified model parameters for an origami Kresling tower. It is clear that the model accurately describes the folding process. Thus, the model can provide an accurate prediction of folding kinematic at certain creases. Consequently, technical requirements, such as final folding angle and criteria force on the specific crease, can be accurately investigated using the proposed model.

For the current configuration of the origami type Kresling tower, the bistable fold/deployment requires a bi-directional actuation force of 23 N with a translation stroke of 20 mm or of a torque of 0.43 Nm with a rotational stroke of 60 degrees. Practically speaking, the actuator needs to be sufficiently compact to be integrated in the structure. Moreover, the translation actuation requires a stroke equivalent to

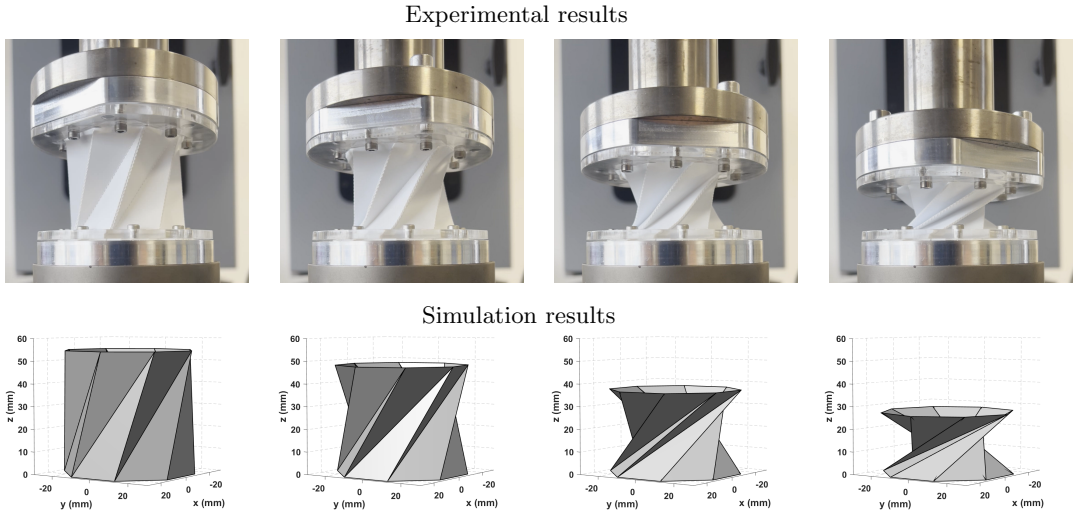

Figure 9: An example of the folding process comparison according to Origami Kresling tower: The photos on top show the incremental state during folding. The images show the simulation results according to corresponding displacements. The model can provide an accurate description of the folding kinematic of structure.

37% of its fully deployed length. Beyond the aforementioned conventional actuation methods, smart materials like shape memory alloys are excellent candidates thanks to their unique advantages in terms of high energy density with large recoverable strain. However, SMA-based tensile wires usually require a length up to 25 times higher than their intended stroke length [9]. A spring can increase the stroke while reducing the output force [15]. On the other hand, torsional actuators provide better potential for such structures according to the stroke requirement [48]. For instance, millimeter-sized bending SMAs can provide a BRM motion with $\pm$ 100 degrees [49], and two torsional SMAs can provide a BRM motion with a stroke up to $\pm$ 180 degrees in the similar scale [50].

Finally, multi-stable structures can be obtained by combining multiple modular Kresling towers whose deformation can be controlled by one single dof actuation. Prior works uses different geometrical parameters [28, 27, 22] or different materials [13] to obtain distinct energy barrier according to folding. Consequently, each element induces individual criteria force for folding and deployment, enabling a controllable multi-stable structure driven by a 'loading-path' depending model. However, the change of the geometrical parameters induces variations in criteria force and bistable portion simultaneously, while a modification on the mount creases induces a large variation of criteria force with a limited impact on the bistable portion. Therefore, further research on strategies focused on the control of crease is required to obtain simple and efficient design of Kresling tower-based multifunctionnal origami robots.

4. Conclusion

This paper presents a method to obtain the technical requirements for the actuation of non-rigid origami fabricated by engineering material. The proposed method is applied to PP-based Kresling tower. Two versions (origami and kirigami) of Kresling tower are thoroughly characterized using three experiments. The results of the origami stabilization test show that a Kresling tower using PP requires at least two hundred full folding and deployment cycles to provide a repeatable mechanical response. The BRM test address the stabilized mechanical and kinematic behavior during the shape-changing of two well-known origami types regarding the same geometric design. The results show the opening of mountain creases induces modifications to the Kresling tower's global mechanical performance while observing the distinct coupling relationships between rotation and translation. The actuation test results show that the structure's shape-changing requires not only the criteria force but also the final folding angle to achieve the bistable shape-changing. Toward the actuation of origami robot using PP-based Kresling tower, three technical requirements are identified for 'self-actuation' application: 1) threshold torque for folding, 2) shape-blocking stiffness for folding, and 3) bistable portion that rely on the actuators output limits of both effort and stroke. Besides the experimental approach, a numerical model using the 'bar-hinge' approach is proposed to describe the crease releasing on the three criteria demands for BRM actuator. The model is demonstrated sufficient for the actuation technical requirement construction while offering a precise prediction of folding kinematic. Perspectives can be: 1) quantitative investigation of the influence releasing of the mountain crease to structure's mechanical performance, 2) development of an origami robot using PP-based non-rigid origami, and 3) enrichment of the 'bar-hinge' model for thick-material-based origami.

5. Acknowledgement

This work was supported by the French National Agency for Research (OrigaBot ANR-18-CE33-0008), and EUR EIPHI (Contract No. ANR-17-EURE-0002).

[1] Li S, Fang H, Sadeghi S, Bhovad P and Wang K W *Advanced Materials* **31** 1805282 (*Preprint* https://onlinelibrary.wiley.com/doi/pdf/10.1002/adma.201805282) URL https://onlinelibrary.wiley.com/doi/abs/10.1002/adma.201805282

[2] Suzuki H and Wood R J 2020 *Nature Machine Intelligence* **2** 437–446 ISSN 2522-5839 URL http://www.nature.com/articles/s42256-020-0203-4

[3] Benouhiba A, Rougeot P, Andreff N, Rabenorosoa K and Ouisse M 2021 *Smart Materials and Structures* URL https://doi.org/10.1088/1361-665x/abe180

[4] Morgan J, Magleby S P and Howell L L 2016 *Journal of Mechanical Design* **138** ISSN 1050-0472 052301 (*Preprint* https://asmedigitalcollection.asme.org/mechanicaldesign/article-pdf/138/5/052301/6228121/md_138_05_052301.pdf) URL https://doi.org/10.1115/1.4032973

[5] Zhakypov Z, Mori K, Hosoda K and Paik J 2019 **571** 381–386 ISSN 0028-0836, 1476-4687 URL http://www.nature.com/articles/s41586-019-1388-8

[6] Melancon D, Gorissen B, García-Mora C J, Hoberman C and Bertoldi K 2021 *Nature* **592** 545–550 ISSN 0028-0836, 1476-4687 URL http://www.nature.com/articles/s41586-021-03407-4
[7] Fang H, Chu S C A, Xia Y and Wang K W 2018 *Advanced Materials* **30** 1706311 ISSN 0935-9648, 1521-4095 URL https://onlinelibrary.wiley.com/doi/10.1002/adma.201706311
[8] Lee Dae-Young, Kim Jae-Kyeong, Sohn Chang-Young, Heo Jeong-Mu and Cho Kyu-Jin 2021 *Science Robotics* **6** eabe0201 publisher: American Association for the Advancement of Science URL https://doi.org/10.1126/scirobotics.abe0201
[9] Hu K, Rabenorosoa K and Ouisse M 2021 *Frontiers in Robotics and AI* **8** 678486 ISSN 2296-9144 URL https://www.frontiersin.org/articles/10.3389/frobt.2021.678486/full
[10] Rus D and Tolley M 2018 *Nature Reviews Materials* **3** 101–112
[11] Reid A, Lechenault F, Rica S and Adda-Bedia M 2017 *Phys. Rev. E* **95**(1) 013002 URL https://link.aps.org/doi/10.1103/PhysRevE.95.013002
[12] Turner N, Goodwine B and Sen M 2016 *Proceedings of the Institution of Mechanical Engineers, Part C: Journal of Mechanical Engineering Science* **230** 2345–2362 URL https://doi.org/10.1177/0954406215597713
[13] Melancon D, Forte A E, Kamp L M, Gorissen B and Bertoldi K 2022 *Advanced Functional Materials* 2201891 ISSN 1616-301X, 1616-3028 URL https://onlinelibrary.wiley.com/doi/10.1002/adfm.202201891
[14] Faber J A, Arrieta A F and Studart A R 2018 *Science* **359** 1386–1391 ISSN 0036-8075, 1095-9203 URL https://www.science.org/doi/10.1126/science.aap7753
[15] Fang H, Zhang Y and Wang K W 2017 *Bioinspiration & Biomimetics* **12** 065003 ISSN 1748-3190 URL https://iopscience.iop.org/article/10.1088/1748-3190/aa8448
[16] Grey S W, Scarpa F and Schenk M 2021 *Journal of Mechanical Design* **143** ISSN 1050-0472 081703 URL https://doi.org/10.1115/1.4049880
[17] Meloni M, Cai J, Zhang Q, Lee D S H, Li M, Ruijun M, Parashkevov T and Feng J 2021 *Advanced Science* **8**
[18] Benouhiba A 2020 *Structures actives à base d'origami pour des résonateurs de Helmholtz adaptatifs et la robotique souple* Ph.D. thesis thèse de doctorat dirigée par Andreff, Nicolas Ouisse, Morvan et Rabenorosoa, Kanty Automatique Bourgogne Franche-Comté 2020 URL http://www.theses.fr/2020UBFCD011
[19] Guest S D and Pellegrino S 1994 *Journal of Applied Mechanics* **61** 773–777 ISSN 0021-8936 (*Preprint* https://asmedigitalcollection.asme.org/appliedmechanics/article-pdf/61/4/773/5464016/773_1.pdf) URL https://doi.org/10.1115/1.2901553
[20] Biruta K 2008 Natural twist buckling in shells: from the hawkmoth's bellowstothe deployable kresling-patternand cylindrical miura-ori *Proceedings of the 6th International Conference onComputation of Shell and Spatial Structures*
[21] Lang R J 2017 *Twists, tilings, and tessellations: Mathematical methods for geometric origami* (CRC Press)
[22] Jules T 2020 *Géométrie et Mécanique des Origamis* Ph.D. thesis thèse de doctorat dirigée par Adda-Bedia, Mokhtar et Lechenault, Frédéric Physique Lyon 2020 URL http://www.theses.fr/2020LYSEN060
[23] Sargent B, Butler J, Seymour K, Bailey D, Jensen B, Magleby S and Howell L 2020 *Journal of Mechanisms and Robotics* **12** ISSN 1942-4302 041005 URL https://doi.org/10.1115/1.4045846
[24] Ishida S, Uchida H, Shimosaka H and Hagiwara I 2017 *Journal of Vibration and Acoustics* **139** ISSN 1048-9002 031015 URL https://doi.org/10.1115/1.4036096
[25] Pagano A, Yan T, Chien B, Wissa A and Tawfick S 2017 *Smart Materials and Structures* **26** 094007 URL https://doi.org/10.1088/1361-665x/aa721e
[26] Kaufmann J, Bhovad P and Li S 0 *Soft Robotics* **0** null pMID: 33769099 (*Preprint* https://doi.org/10.1089/soro.2020.0075) URL https://doi.org/10.1089/soro.2020.0075
[27] Novelino L, Ze Q, Wu S, Paulino G and Zhao R 2020 *Proceedings of the National Academy of*

Sciences of the United States of America **117**

[28] Nayakanti N, Tawfick S H and Hart A J 2018 *Extreme Mechanics Letters* **21** 17–24 ISSN 2352-4316 URL https://www.sciencedirect.com/science/article/pii/S2352431617300998

[29] Filipov E, Liu K, Tachi T, Schenk M and Paulino G 2017 *International Journal of Solids and Structures* **124** 26–45 ISSN 0020-7683 URL https://www.sciencedirect.com/science/article/pii/S0020768317302408

[30] Jianguo C, Xiaowei D, Yuting Z, Jian F and Ya Z 2016 *Journal of Mechanisms and Robotics* **8**

[31] Kidambi N and Wang K W 2020 *Physical Review E* **101** 063003 ISSN 2470-0045, 2470-0053 URL https://link.aps.org/doi/10.1103/PhysRevE.101.063003

[32] Li Z, Kidambi N, Wang L and Wang K W 2020 *Extreme Mechanics Letters* **39** 100795 ISSN 23524316 URL https://linkinghub.elsevier.com/retrieve/pii/S2352431620301140

[33] Masana R and Daqaq M F 2019 *Phys. Rev. E* **100**(6) 063001 URL https://link.aps.org/doi/10.1103/PhysRevE.100.063001

[34] Liu K and Paulino G 2018 Highly efficient nonlinear structural analysis of origami assemblages using the merlin2 software *Proceedings from the seventh meeting of Origami, Science, Mathematics and Education* vol 3 pp 1167–1182

[35] Liu K and Paulino G 2017 *Proceedings of the Royal Society A: Mathematical, Physical and Engineering Science* **473** 20170348

[36] 2016 *Highly Compressible Origami Bellows for Harsh Environments* (*International Design Engineering Technical Conferences and Computers and Information in Engineering Conference* vol Volume 5B: 40th Mechanisms and Robotics Conference) v05BT07A001 (*Preprint* https://asmedigitalcollection.asme.org/IDETC-CIE/proceedings-pdf/IDETC-CIE2016/50169/V05BT07A001/4261466/v05bt07a001-detc2016-59060.pdf) URL https://doi.org/10.1115/DETC2016-59060

[37] Sargent B, Butler J, Seymour K, Bailey D, Jensen B, Magleby S and Howell L 2020 *Journal of Mechanisms and Robotics* **12** ISSN 1942-4302 041005 (*Preprint* https://asmedigitalcollection.asme.org/mechanismsrobotics/article-pdf/12/4/041005/6493664/jmr_12_4_041005.pdf) URL https://doi.org/10.1115/1.4045846

[38] Guest S D and Pellegrino S 1996 *Journal of Applied Mechanics* **63** 77–83 ISSN 0021-8936 (*Preprint* https://asmedigitalcollection.asme.org/appliedmechanics/article-pdf/63/1/77/5464717/77_1.pdf) URL https://doi.org/10.1115/1.2787212

[39] Bhovad P, Kaufmann J and Li S 2019 *Extreme Mechanics Letters* **32** 100552 ISSN 2352-4316 URL https://www.sciencedirect.com/science/article/pii/S2352431619302202

[40] Berre J, Geiskopf F, Rubbert L and Renaud P 2021 Towards a Synthesis Method of Kresling Tower Used as a Compliant Building Block (*International Design Engineering Technical Conferences and Computers and Information in Engineering Conference* vol Volume 8B: 45th Mechanisms and Robotics Conference (MR)) v08BT08A038 (*Preprint* https://asmedigitalcollection.asme.org/IDETC-CIE/proceedings-pdf/IDETC-CIE2021/85451/V08BT08A038/6801187/v08bt08a038-detc2021-68904.pdf) URL https://doi.org/10.1115/DETC2021-68904

[41] Sareh P, Chermprayong P, Emmanuelli M, Nadeem H and Kovac M 2018 *Science Robotics* **3** eaah5228

[42] Francis K C, Blanch J E, Magleby S P and Howell L L 2013 *Mechanical Sciences* **4** 371–380 URL https://ms.copernicus.org/articles/4/371/2013/

[43] Zhang Q, Fang H and Xu J 2021 *Frontiers in Robotics and AI* **8** 271 ISSN 2296-9144 URL https://www.frontiersin.org/article/10.3389/frobt.2021.738214

[44] Yasuda H, Tachi T, Lee M and Yang J 2017 *Nature Communications* **8**(1) 962 URL https://doi.org/10.1038/s41467-017-00670-w

[45] Wagner M A, Huang J L, Okle P, Paik J and Spolenak R 2020 *Materials & Design* **191** 108643 ISSN 0264-1275 URL https://www.sciencedirect.com/science/article/pii/S0264127520301775

[46] Vaiana N, Sessa S and Rosati L 2021 *Mechanical Systems and Signal Processing* **146** 106984 ISSN 0888-3270 URL https://www.sciencedirect.com/science/article/pii/S0888327020303708

[47] Richaud E, Fayolle B and Davies P 2018 14 - tensile properties of polypropylene fibers *Handbook of Properties of Textile and Technical Fibres (Second Edition)* The Textile Institute Book Series ed Bunsell A R (Woodhead Publishing) pp 515–543 second edition ed ISBN 978-0-08-101272-7 URL https://www.sciencedirect.com/science/article/pii/B9780081012727000146

[48] Hu K, Ouisse M and Rabenorosoa K 2022 Design of a bidirectional rotational motion actuator by sma with geometrico-static requirements *XVI SPIE Behavior and Mechanics of Multifunctional Materials and Composites (2022)* vol 12044 (Californie, United States) p 1204405 (12)

[49] Kim Y, Jang T, Gurung H, Mansour N A, Ryu B and Shin B 2019 *Sensors and Actuators A: Physical* **295** 512–522

[50] Kim S, Lee D, Koh J and Cho K 2016 Fast, compact, and lightweight shape-shifting system composed of distributed self-folding origami modules *2016 IEEE International Conference on Robotics and Automation (ICRA)* pp 4969–4974